

TECHNICAL REPORT 1945  
August 2006

**Advanced Propagation Model (APM)  
Analysis of VHF Signals in the  
Southern California Desert**

A. E. Barrios  
K. D. Anderson  
G. E. Lindem

Approved for public release;  
distribution is unlimited.

SSC San Diego

TECHNICAL REPORT 1945  
August 2006

# **Advanced Propagation Model (APM) Analysis of VHF Signals in the Southern California Desert**

A. E. Barrios  
K. D. Anderson  
G. E. Lindem

Approved for public release;  
distribution is unlimited.



SSC San Diego  
San Diego, CA 92152-5001

**SSC SAN DIEGO**  
**San Diego, California 92152-5001**

---

---

**F. D. Unetic, CAPT, USN**  
Commanding Officer

**C. A. Keeney**  
Executive Director

**ADMINISTRATIVE INFORMATION**

The work described in this report was prepared for the Office of Naval Research Ocean, Atmosphere and Space Research Division's Marine Meteorology & Atmospheric Effects Program (ONR 322MM) by the Atmospheric Propagation Branch (Code 2858) of SPAWAR Systems Center San Diego (SSC San Diego).

Released by  
T. Tsintikidis, Head  
Atmospheric Propagation Branch

Under authority of  
S. Russell, Head  
Electromagnetics & Advanced  
Technology Division

This is a work of the United States Government and therefore is not copyrighted. This work may be copied and disseminated without restriction. Many SSC San Diego public release documents are available in electronic format at <http://www.spawar.navy.mil/sti/publications/pubs/index.html>

**ACKNOWLEDGMENTS**

The authors wish to thank Professor Kent Chamberlin from the University of New Hampshire for his insightful discussions; Mr. Gary Banks from the NOAA for confirmation of the weather radio transmitter Global Positioning System coordinates and elevations used in this analysis; <http://data.geocomm.com/> for making freely available USGS DEM data; and finally, special thanks to Richard Horne for creating and making available his 3DEM software (<http://www.visualizationsoftware.com/3dem.html>).

## **EXECUTIVE SUMMARY**

### **OBJECTIVE**

This report analyzes very high frequency signal strength data from two Naval Oceanic & Atmospheric Administration weather radio transmitters located in southern California and southwestern Arizona over a wide range of topography ranging from relatively flat to mountainous terrain. Meteorological information was obtained from local radiosonde measurement stations at Miramar (NKX) and Yuma Proving Ground (1Y7). These data are used as the basis for a validation study of the Advanced Propagation Model (APM) to determine its applicability for low-altitude mobile radio communications applications over terrain.

### **RESULTS**

The APM performs very well for low-altitude propagation over terrain and at least as well as the widely used diffraction model, TIREM, under standard conditions. The APM performs better when variable refractivity data are available.

# CONTENTS

<b>EXECUTIVE SUMMARY</b> .....	<b>iii</b>
<b>I. INTRODUCTION</b> .....	<b>1</b>
<b>II. MEASUREMENTS</b> .....	<b>3</b>
A. RADIO DATA .....	3
B. METEOROLOGICAL DATA .....	5
C. TERRAIN .....	9
<b>III. RESULTS</b> .....	<b>13</b>
A. WXL-87 (YUMA).....	14
B. KEC-62 (SAN DIEGO) .....	18
C. 30 JUNE 2004 .....	24
<b>IV. DISCUSSION</b> .....	<b>29</b>
<b>V. CONCLUSION</b> .....	<b>31</b>
<b>VI. REFERENCES</b> .....	<b>33</b>

## Figures

1. The receiver antenna mounted on a pickup truck (a) and the receiver with laptop computer in the truck (b).....	4
2. Terrain elevation map of San Diego and Imperial counties, southern California.....	5
3. Percent occurrence of (a) surface-based ducts and (b) elevated ducts in San Diego, California, based on the GTE Sylvania climatological database .....	7
4. Soundings from meteorological station NKX, along with surface-based duct and elevated duct profiles constructed from climatology for the corresponding observation months .....	7
5. Percent occurrence of surface-based ducts in Yuma, Arizona, based on the GTE Sylvania climatological database .....	8
6. Soundings from meteorological station 1Y7, along with surface-based duct profiles constructed from climatology for the corresponding observation months .....	9
7. Terrain elevation profile from the KEC-62 transmitter location to the easternmost receiver point on 04 Dec 03 .....	10
8. Difference in terrain elevation between USGS and DTED terrain at the coordinates of the receiver for the (a) KEC-62 transmitter indicated by the white curve in Figure 2, and (b) for the WXL-87 transmitter indicated by the magenta curve in Figure 2 .....	11
9. Separation of receiver coordinates for KEC-62 east of the longitude position (black) and receiver coordinates west of the longitude position (red).....	11
10. Observed signal strength from WXL-87 transmitter on 09 June 2004 and APM predictions for various profiles from sounding and climatology (solid colored lines) using terrain information from USGS (top) and DTED (bottom).....	14

11. RMS error between measurements and APM predictions for each measurement day for the WXL-87 transmitter. APM predictions were obtained based on USGS terrain data, and refractivity profiles are applied relative to mean sea level (solid line) and relative to the ground height along the path (dashed line) .....	15
12. RMS error between measurements and APM predictions for each measurement day for the WXL-87 transmitter. Predictions were obtained using DTED (solid line) and USGS (dashed line) information. All refractivity profiles are applied relative to the local ground height along the path .....	17
13. 95% confidence interval of observations (shaded area in all plots) along with (a) the observed mean, (b) the APM predictions, and (c) the TIREM predictions (all shown as black lines) from the WXL-87 transmitter as a function of range from the transmitter. APM and TIREM predictions based on standard atmosphere and USGS terrain.....	18
14. Observed signal strength from the KEC-62 transmitter on 23 June 2004 and the APM predictions for various profiles from soundings, climatology, and standard atmosphere (green line most easily seen) using terrain information from USGS (top) and DTED (bottom).....	19
15. RMS error between measurements and APM predictions for each measurement for the KEC-62 transmitter. APM predictions were obtained based on USGS terrain data, and refractivity profiles are applied relative to msl (solid line) and relative to the local ground height along the path (dashed line).....	20
16. RMS error between measurements and the APM predictions for each measurement day for the KEC-62 transmitter. Predictions were obtained using DTED (solid line) and USGS (dashed line) information. All refractivity profiles are applied relative to the local ground height along the path.....	21
17. 95% confidence interval (shaded area) and mean (black line) of observations from the KEC-62 transmitter for portions of the receiver route (a) west and (b) east of the transmitter, indicated by the red and black curves, respectively, shown in Figure 9 .....	22
18. 95% confidence interval as in Figure 17 (shaded area), along with the mean of the APM predictions (black line) for the KEC-62 transmitter for portions of the receiver route (a) west and (b) east of the transmitter, based on standard atmosphere and USGS terrain .....	23
19. 95% confidence interval as in Figure 17 (shaded area), along with the mean of the TIREM predictions (black line) for the KEC-62 transmitter for portions of the receiver route (a) west and (b) east of the transmitter, based on standard atmosphere and USGS terrain .....	23
20. Southern California coastal area showing locations of KIH-34 (Santa Barbara) and KEC-62 (San Diego) transmitters. Magenta portion of the receiver route indicates where KIH-34 transmissions were received on 30 June 2004.....	24
21. Signal strength received on 23 June 2004 from the KEC-62 transmitter (black) and on 30 June 2004 from the KIH-34 transmitter (red) along the identical portion of the receiver route (magenta curve in Figure 20) .....	25
22. Miramar (NKX) and Vandenberg (VBG) soundings for 30 June 2004.....	26
23. KIH-34 observed signal strength on 30 June 2004 and predictions from the APM using VBG and NKX soundings and DTED terrain .....	27

## Tables

1. NOAA weather radio transmitters .....	3
2. Available radiosonde measurements .....	6
3. WXL-87 (USGS terrain) .....	16
4. KEC-62 APM RMS error in dBm (USGS terrain, refractivity applied relative to ground) ....	21
5. KEC-62 APM standard deviation in dBm (USGS terrain).....	22

# I. INTRODUCTION

Many validation studies have been conducted of tropospheric radiowave propagation models and their ability to adequately predict propagation loss at low altitudes for frequencies from very high frequency (VHF) to Ku-band over various terrain [1]–[4], sea [5]–[8], and mixed land/sea paths [9], [10]. Validation studies on propagation data collected for over-water paths focused on the effects of anomalous propagation conditions such as elevated and surface-based ducts—particularly evaporation ducts, which are prevalent over the ocean [11], [12].

Of course, propagation data collection on over-terrain paths has been much more extensive; however, these validation studies focused primarily on terrain and not atmospheric effects [13]. Indeed, many of the widely used models designed primarily for propagation over land ignore horizontal and vertical variations in the refractive profile and instead rely on a single linear gradient (equivalently an effective earth radius factor) to describe the lower atmosphere [2], [14]. Therefore, most data collections reported in the open literature contain only propagation data and lack corresponding meteorological measurements.

These authors are aware of only one over-terrain data set that contains both radio propagation data and an extensive set of refractive profile measurements made along the propagation path. The measurement campaign was conducted by our predecessor propagation group at (what was then called) the Naval Electronics Laboratory [15]. A transmitter was located at Gila Bend, Arizona, with two receiver stations along the path, one located 26.7 miles from the emitter and the second located over 46 miles from the same emitter. Transmitting and receiving antennas were mounted on 200-ft towers using an elevator system that allowed signal height-gain measurements from the surface to 200 ft in height for various pre-selected antenna heights at the transmitter tower. Meteorological measurements were made at the terminal stations and several other stations along the path, which showed low-lying, surface-based ducts forming in the early morning hours due to radiational cooling from the desert floor.

This radio propagation data set, taken over terrain that includes measured range-dependent refractive profiles showing surface-based ducts of varying thickness along the propagation path, was one of the first data sets used in validating our propagation model [16]. The model showed good agreement with observations and this particular data set showed, above all, that once heights are approached above the terrain where diffraction is not the dominant propagation mechanism, the refractivity does indeed significantly impact the field strength and one cannot assume simple standard atmosphere conditions.

The model described in Reference [16] was the predecessor to our current Advanced Propagation Model (APM), which is the model discussed in this report. APM is based on the split-step Fourier parabolic equation (PE) algorithm and has been funded primarily by the Office of Naval Research for operational use by the U.S. Navy. It was initially developed to model anomalous and range-dependent atmospheric effects on radiowave propagation over the ocean. However, with Navy operational requirements focusing on the littoral environment in the last 10 to 15 years, there was a strong need to accommodate range-dependent refractive profiles along with terrain effects. Therefore, APM has been improved over the years to also model terrain effects for propagation over land. For a detailed description of the algorithms within APM and the history of its development, see Reference [17].

A common feature in previous propagation data sets taken over land is that both terminal points are usually fixed, or as in the case with the Arizona data in Reference [15], the terminals are at fixed ranges from one another, but variable in height. Simultaneous meteorological measurements are rare. The primary focus of the validation study discussed in this report is to assess how well APM performs for low-altitude transmitter/receiver geometries over land where the receiver is *mobile* and where some measure of the refractivity is known via local radiosonde stations. The APM is a hybrid ray optics/PE model that is described in detail in Reference [17]. Also see Reference [18] for additional derivations on alternative PE models, along with references to various data collection campaigns.

The secondary purpose of this validation study is to quantify errors between observed and predicted field strength values produced by commonly used terrain databases within the United States. Before the existence of the Digital Terrain Elevation Database (DTED) or the United States Geological Survey (USGS) database, characterizing the terrain elevation profile along a particular propagation path was difficult because terrain elevation profiling was manual. With these databases now readily available, a more complete validation study on propagation models is possible. Having ready access to databases such as DTED or USGS allows the model to ingest multiple terrain elevation profiles, providing signal strength coverage for multiple receiver/target locations fairly quickly.

Section II discusses the experimental setup and the radio signal strength measurements, along with the environmental information applied in the analysis. Section III presents the results of the APM performance with observations, as well as the performance of a widely used terrain diffraction model, the Terrain Integrated Rough Earth Model (TIREM) [14].

## II. MEASUREMENTS

### A. RADIO DATA

Our signals of opportunity for the propagation data are two National Oceanic & Atmospheric Administration (NOAA) weather radio transmitters. The two transmitters are located in San Diego, California (station call sign KEC-62), and near Yuma, Arizona (station call sign WXL-87). The system parameters and coordinate locations for both transmitters are listed in Table 1.

Table 1. NOAA weather radio transmitters.

	San Diego KEC-62	Yuma WXL-87
Frequency (MHz)	162.4	162.55
Power (watts)	100	100
Elevation above mean sea level (msl) (meters)	882.9	666.2
Elevation relative to ground (rtg) (meters)	99.7	90.5
Location coordinates (latitude/longitude)	33N 00' 32"/ 116W 58' 02"	33N 03' 17"/ 114W 49' 33"

The VHF measurement system consists of an ICom 8500 radio to measure received signal power versus time, a Global Positioning System (GPS) unit to determine latitude and longitude versus time, and a laptop computer to control both. The ICom 8500 radio was connected to a quarter-wave dipole antenna that was mounted on the side wall of the bed of a pickup truck, 2.2 m above the surface. Figure 1 shows the VHF antenna and receiver mounted in a truck. In this setup, the 12-V supply for the radio came from the truck battery. A separate car battery powered the laptop. The radio is configured for receiving frequency modulation (12-kHz) signals with automatic frequency control off (to prevent de-tuning the radio under low-signal conditions).

This radio was fixed-tuned to the KEC-62 transmitter (162.4 MHz) or the WXL-87 transmitter (162.55 MHz) with a 12.5-kHz receiver bandwidth. Signal strength data were recorded by monitoring the “*S-meter*” reading that was calibrated to signal power received at the antenna. Calibration was accomplished using a precise Anritsu<sup>®</sup> signal generator feeding the antenna cable connected to the ICom 8500 receiver, both tuned to 162.4 MHz. Input power levels were varied from  $-115$  to  $-20$  dBm, and 20 samples were taken at each level (sampled at 1-s intervals), which were averaged and recorded as one reading. Standard deviation of the 20 *S-meter* samples was less than 1 *S-meter* unit, typically zero, for inputs of  $-20$  to  $-90$  dBm. The ICom 8500 radio was calibrated before each measurement, and was consistent. A calibration dependency on input voltage to the radio was noted and the input voltage was monitored during each measurement. The dipole antenna is assumed to contribute a 2.3-dBi gain. No antenna patterns for an antenna mounted on the truck were made; a repeatable (per measurement) dipole pattern is assumed. Simultaneously, latitude and longitude in WGS-84 coordinates were recorded by monitoring a Garmin<sup>®</sup> model 48 GPS receiver.



Figure 1. The receiver antenna mounted on a pickup truck (a) and the receiver with laptop computer in the truck (b).

Radio signal strength and GPS latitude/longitude coordinates were measured at the receiver as the vehicle traveled eastward on Interstate 8 from the Space and Naval Warfare Systems (SPAWAR) Center San Diego (SSC San Diego) facility to less than 50 km from the WXL-87 transmitter. Radio signals were measured along the outbound (traveling east) and inbound (traveling west) routes over the course of 10 days, from 4 December 2003 to 1 July 2004. Average observation time for the complete round-trip was roughly 5 hours for each day. The receiver route spans the San Diego and Imperial counties and is illustrated in the terrain elevation map in Figure 2. The yellow crosses show the locations of NOAA transmitters. That portion of the measurement route shown in white indicates where signals from the KEC-62 transmitter were recorded, and that portion of the route shown in magenta indicates where signals from the WXL-87 transmitter were recorded. The location illustrating the “switch” from recording the KEC-62 signals to the WXL-87 signals was fairly typical for the outbound and inbound runs, and for each day varied to within a few kilometers.

On the first measurement day, 04 Dec 2003, the signal strength was initially recorded based on 30-s averages of 5-s samples. For the remaining measurement days, the signal strength was sampled and recorded at 1-s intervals. Also, on day 03 Feb 2004, data collected from the KEC-62 transmitter was available from the westbound direction of the receiver route only.

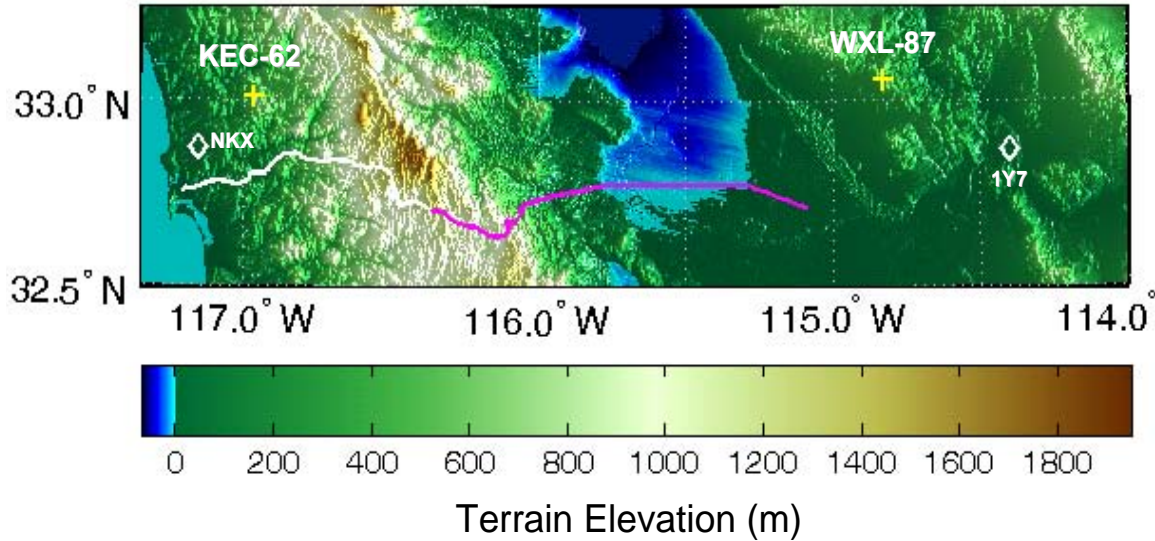


Figure 2. Terrain elevation map of San Diego and Imperial counties, southern California. The location of the NOAA transmitters (KEC-62 and WXL-87) are indicated by yellow crosses (+). The location of the radiosonde stations (NKX and 1Y7) are indicated by white diamonds ( $\diamond$ ). The white receiver route indicates where signals were measured from the KEC-62 transmitter and the magenta receiver route indicates where signals from the WXL-87 transmitter were measured for each of the 10 days.

## B. METEOROLOGICAL DATA

The meteorological information used for the model predictions were taken from both real-time radiosonde measurements and climatology.

Soundings were obtained from two meteorological stations, one located at the Marine Corps Air Station, Miramar (NKX), in San Diego, and the other located at Yuma Proving Ground (1Y7). The white diamonds in Figure 2 indicate the locations of these stations. While obtaining soundings at the transmitter sites and other locations along the propagation paths would have been more desirable, obtaining soundings was impossible for several reasons, the main reason being logistics. As shown in Figure 2, much of the area just east of San Diego is mountainous and cannot be reached by car. Applying soundings from station 1Y7 may also be considered a “stretch” because of its distance from station WXL-8; however, station 1X7 is the nearest meteorological station to the WXL-87 transmitter site. Also, any formation of surface-based ducts in the desert area is more often caused by thermal cooling, and since the topology is very similar at both locations, any occurrence of surface-based ducts from soundings at the 1Y7 location would provide useful information for the area surrounding WXL-87, so we chose not to omit these soundings.

Radiosondes are normally launched twice each day at 0000Z and 1200Z, which corresponds locally to 1600 Pacific Standard Time (PST) and 0400 PST, respectively, during the winter months; and 1700 Pacific Daylight Time (PDT) and 0500 PDT, respectively, during the summer months. Based on Zulu time, the local daytime sounding at 1600 PST would correspond to time 0000Z recorded for the following day. Therefore, to avoid confusion, Table 2 lists days when radio signal measurements were recorded, along with *local* times of available soundings obtained at both meteorological stations for all 10 measurement days. Radiosondes launched from meteorological station 1Y7 were sporadic and did not strictly follow the 12-hour interval schedule.

Table 2. Available radiosonde measurements.

Data Collection Days	Miramar (NKX)	Yuma Proving Ground (1Y7)
04 Dec 03	0400, 1600 PST	0400 PST
03 Feb 04	0400, 1600 PST	1500 PST
06 Apr 04	0500, 1700 PDT	0500 PDT
07 Apr 04	0500, 1700 PDT	0400 PDT
27 May 04	0500, 1700 PDT	0500, 1100 PDT
09 Jun 04	0500, 1700 PDT	0500 PDT
23 Jun 04	0500, 1700 PDT	0500 PDT
24 Jun 04	0500, 1700 PDT	0500, 1100 PDT
30 Jun 04	1700 PDT	0500 PDT
01 Jul 04	0500, 1700 PDT	0500 PDT

Due to the sparseness of real-time soundings, we also used climatology from the GTE Sylvania climatological database. The database is based on a large-scale analysis of approximately 3 million worldwide radiosonde soundings from 921 observing stations over a 5-year period [19]. Statistics of tropospheric ducts and super-refractive layers are available from this database and vertical refractive profiles were constructed based on these statistics.

To obtain predictions from the APM for comparisons with the KEC-62 observations, surface-based and elevated ducts were constructed based on San Diego climatology (Figure 3). In San Diego, the percent occurrence of surface-based ducts is fairly high. During the daytime from June through August, the percent occurrence is over 30%, with August at over 40% of the time. During the winter months of December and January, surface-based ducting occurs more often at night. Initially, only surface-based ducts were considered for inclusion in this validation analysis; however, as shown in Figure 3b, the percent occurrence of elevated ducts in San Diego is even higher—at over 50% for more than half of the year, during daytime and nighttime, which is, no doubt, due to the marine influence.

Figure 4 shows refractive profiles computed from soundings for the 10-day observation period and those constructed based on climatology. All profiles are plotted and referenced for mean sea level. The shaded area indicates the actual meteorological station height at Miramar, which is 134 m. Height versus M-unit profiles, computed from soundings obtained at the NKX meteorological station, are shown as solid lines and those based on surface-based and elevated duct climatology are shown as dotted and dashed lines, respectively. Standard atmosphere is also shown for reference. Note that soundings from April through July are consistent with climatology, showing the existence of at least one elevated duct each observation day.

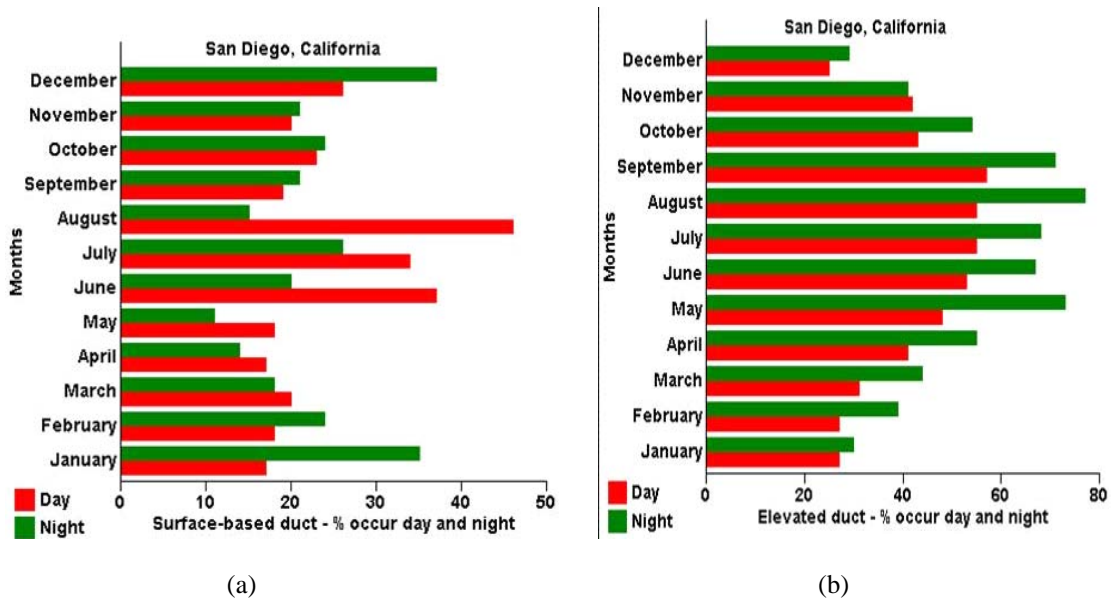


Figure 3. Percent occurrence of (a) surface-based ducts and (b) elevated ducts in San Diego, California, based on the GTE Sylvania climatological database.

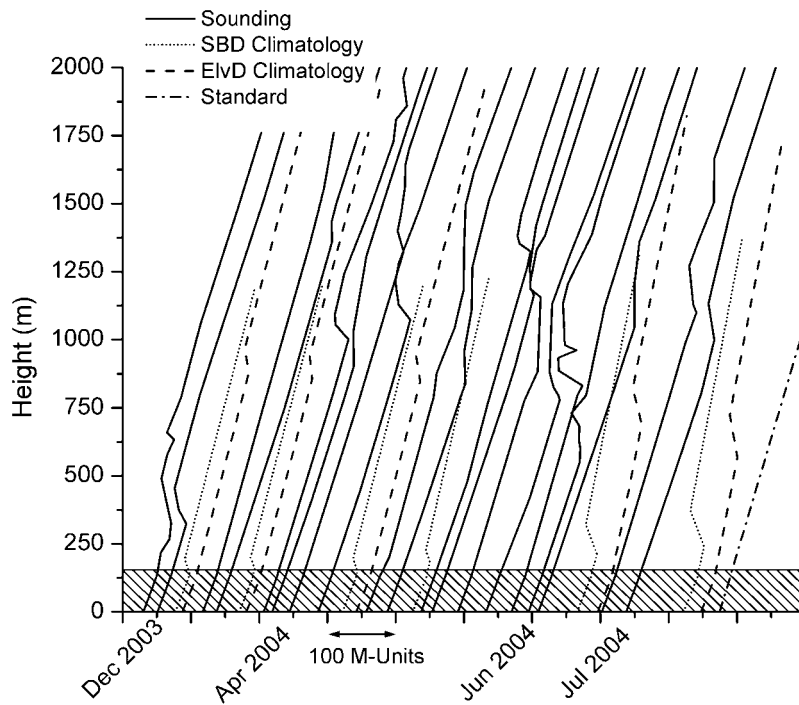


Figure 4. Soundings from meteorological station NKX, along with surface-based duct and elevated duct profiles constructed from climatology for the corresponding observation months. Shaded area represents terrain and indicates meteorological station height.

Figure 5 shows the percent occurrence of surface-based ducts for the Yuma station. Unfortunately, no daytime soundings were available for this area. Overall, surface-based ducting appears to occur far less frequently in this area than in San Diego, with the highest percentage being roughly 24% during September. This percentage seems to contradict the direct meteorological measurements discussed in Reference [15], where surface-based ducts were present on an almost nightly basis (in the early morning hours). However, the number of observations available in the database for this station is less than one-third of that for the San Diego station.

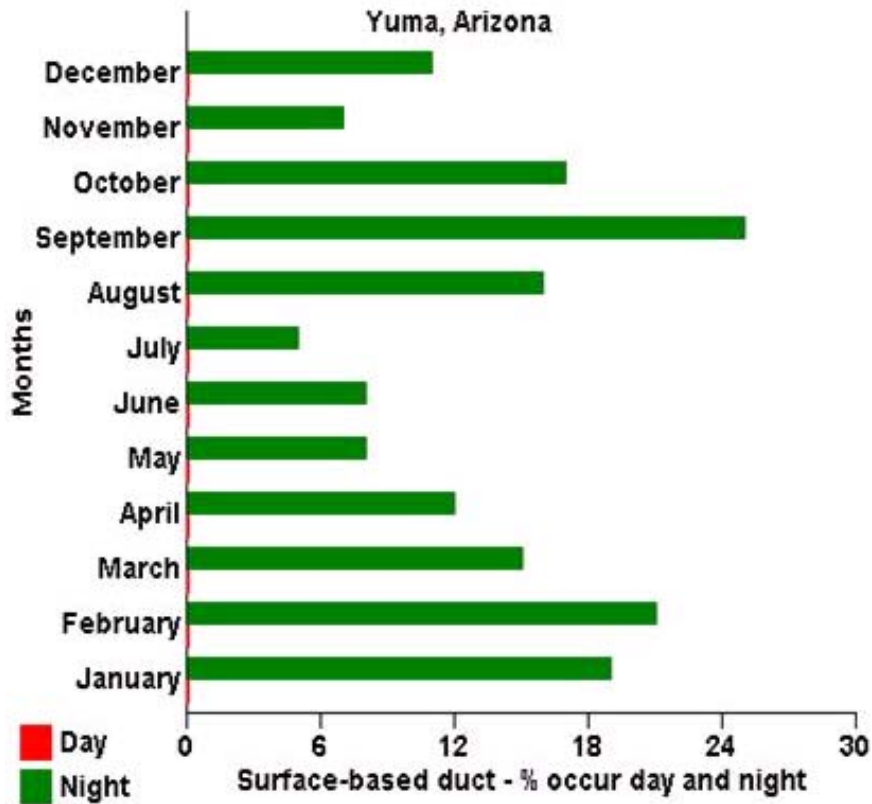


Figure 5. Percent occurrence of surface-based ducts in Yuma, Arizona, based on the GTE Sylvania climatological database.

Figure 6 shows the refractivity profiles from soundings and climatology for the 1Y7 station. Similar to Figure 4, all profiles are plotted relative to mean sea level and the shaded area indicates the height of the 1Y7 station at 131 m. The soundings at this station were of relatively low quality, with many missing levels. Obviously, anomalous propagation conditions were infrequent during this time, a situation that was probably caused by the quality of the soundings at this station. Nevertheless, both soundings and climatology were used in the results presented in Section III.

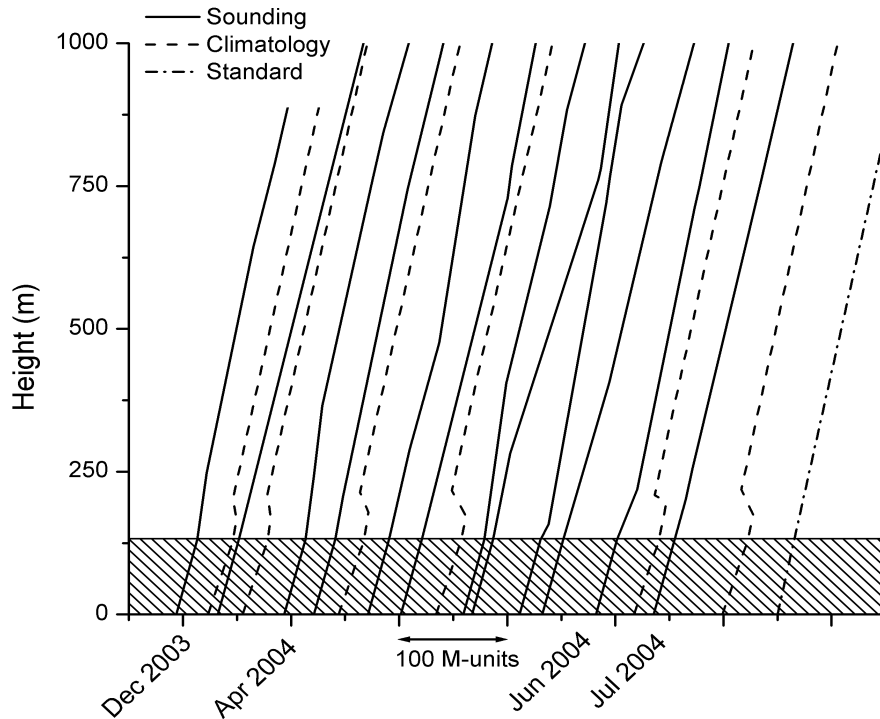


Figure 6. Soundings from meteorological station 1Y7, along with surface-based duct profiles constructed from climatology for the corresponding observation months. Shaded area represents terrain and indicates meteorological station height.

### C. TERRAIN

The second, and perhaps, more significant environmental effect on surface-to-surface propagation over terrain is the variation in elevation of the terrain itself. DTED Level 1 terrain is available for most parts of the world and was initially used to conduct this validation study. Using contour maps as a reference, we quickly discovered problems when confirming the terrain elevation at the NOAA transmitter sites based on DTED information. We next looked at USGS terrain data, which offer a higher resolution. The 7.5-min Digital Elevation Model (DEM) “quadrangles” were the product of choice. Terrain data obtained from DTED Level 1 provide terrain elevation with a horizontal resolution of 100 m and a vertical resolution of  $\pm 30$  m, while the USGS database resolution is 30 m in the horizontal and  $\pm 1$  m in the vertical.

As an example of some of discrepancies we found between DTED and USGS terrain elevation, Figure 7 shows the terrain elevation profile from the KEC-62 transmitter location to the easternmost receiver point for this transmitted signal on day 04 Dec 03 (i.e., the terrain path defined by the yellow cross to the easternmost point of the white curve shown in Figure 2). The terrain elevation values were extracted from DTED and USGS databases (shown as dashed and solid lines, respectively). The

entire terrain profile from the transmitter to the receiver endpoint is roughly 65 km, shown in the insert, with the terrain elevation varying from 500 to over 1600 m. From the plot in the insert, difference in elevation values between the two terrain database sources appears to be almost the same; however, when looking at the first 15 km from the transmitter (larger plot), the difference in elevation is as much as 100 m within the first 5 km from the emitter. This example is just one terrain profile extracted out of thousands necessary to obtain signal strength predictions for each path defined by the transmitter-to-receiver latitude/longitude coordinates along the receiver route in Figure 2.

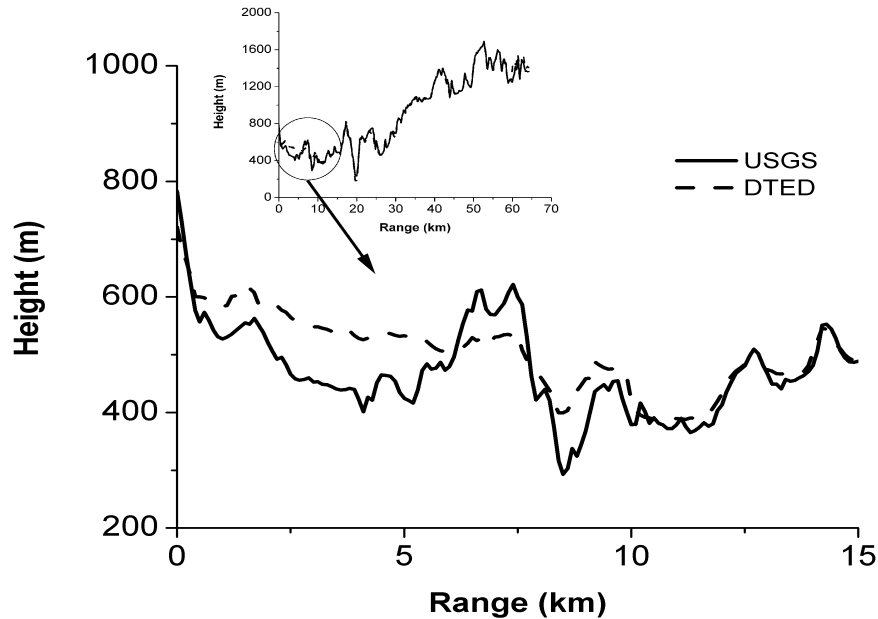


Figure 7. Terrain elevation profile from the KEC-62 transmitter location to the easternmost receiver point on 04 Dec 03. USGS terrain elevation data (solid line) and DTED data (dashed line). Large plot shows the first 15 km of the entire 65-km path (insert).

To illustrate the differences in terrain elevation values between the two database sources, the difference between USGS and DTED terrain elevation at the receiver coordinates recorded on one of the measurement days along the route for the KEC-62 and WXL-87 transmitters are shown in Figure 8a and Figure 8b, respectively. The elevation difference is shown plotted as a function of range from the transmitter. For the KEC-62 receiver route, receiver coordinates with non-unique ranges from the transmitter are plotted because the signal was received east and west of the transmitter longitude. Figure 9 illustrates the portions of the receiver route west of the KEC-62 transmitter, shown in red and corresponding to the red curve in Figure 8a, indicating ranges at which the height differences were computed, while the black curve indicates that portion of the route east of the transmitter longitude, corresponding to the black curve in Figure 8a. Note that for the KEC-62 receiver route, height differences for most of the path fluctuate at roughly  $\pm 20$  m; however, at some ranges, DTED terrain can differ from USGS by as much as 60 m. On the WXL-87 receiver route for ranges close to the transmitter (40 to 100 km), corresponding to the relatively flat area along the route in Figure 2, the height differences do not differ greatly, varying by  $\pm 10$  m, but do approach variations by as much as  $\pm 50$  to 60 m for paths approaching the mountainous terrain on the western portion of the route.

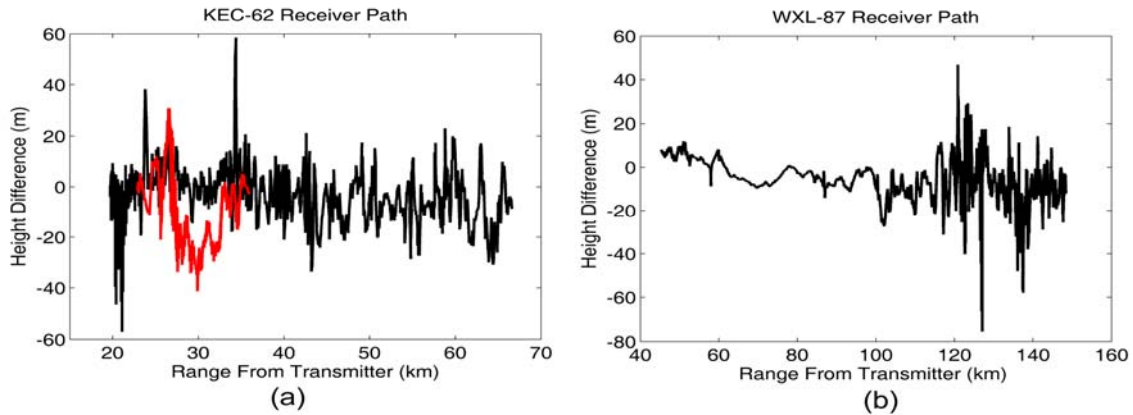


Figure 8. Difference in terrain elevation between USGS and DTED terrain at the coordinates of the receiver for the (a) KEC-62 transmitter indicated by the white curve in Figure 2, and (b) for the WXL-87 transmitter indicated by the magenta curve in Figure 2. The black and red curves in (a) indicate height differences shown for receiver coordinates east and west, respectively, of the KEC-62 longitude as shown in Figure 9.

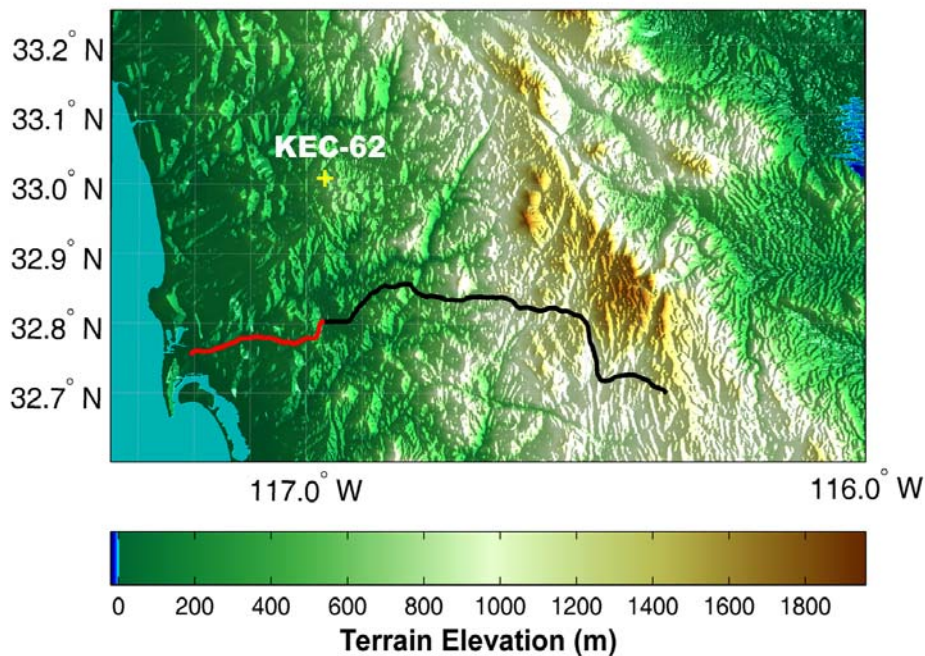


Figure 9. Separation of receiver coordinates for KEC-62 east of the longitude position (black) and receiver coordinates west of the longitude position (red).

The surface properties of the propagation paths from both transmitters to the receiver varied from concrete and asphalt to desert and brush. However, for the KEC-62 paths, more vegetation was present in the form of patchy trees, due to the proximity to the metropolitan area, along with cactus and chaparral as the receiver route extended eastward. The receiver route for the KEC-62 transmitter traversed urban areas where effects from surrounding buildings were not included in the field strength estimations. The route does not include tunnels, but does contain overpasses and bridges, the longest being roughly 600-m long, which overall, should not have a significant effect to alter

the statistical values presented in Section III. The terrain sources used in this analysis did not include foliage or vegetation information as part of the database.

Based on checks for consistency of terrain elevation on selected latitude/longitude coordinates, we view USCG as our reference for the most accurate terrain elevation values. It appears that for the southern California region, DTED may lead to greater error in the elevation values than the vertical resolution in the database would imply. Although USGS has higher vertical resolution, DTED (Level 1) is the terrain database most commonly used within Department of Defense (DoD) for military applications (due to its global coverage), and any operational propagation model used in such applications would in practice be required to use DTED. Therefore, performing a limited sensitivity and validation study of APM using *both* USGS and DTED terrain sources provides a useful measure of the APM's performance, along with quantifying errors one would expect from using a lower resolution terrain source.

The APM results presented in the next section were obtained using the meteorological information previously described in Section II.B and terrain elevation data from DTED and USGS. The USGS DEM quadrangles are referenced to the 1927 North American Datum (NAD27) and the DTED Level 1 data are referenced to the World Geodetic System 1984 (WGS84). Receiver latitude/longitude coordinates recorded via GPS are also referenced to WGS84; therefore, USGS terrain data were appropriately converted and all terrain elevation profiles extracted for signal strength predictions were referenced to WGS84.

### III. RESULTS

The predicted signal strength used in comparisons with measurements are obtained as follows. Both transmitting and receiving antenna gains are assumed to be unity, and vertical polarization is also assumed. The received power in dBm,  $P_r$ , at the antenna is then

$$P_{r(dBm)} = 10 \log P_{t(mW)} - L_{dB}, \quad (1)$$

where  $P_t$  is the transmitter power in mW, and  $L_{dB}$  represents the one-way propagation loss predictions, in dB, obtained from the APM.  $L_{dB}$  is defined as

$$L_{dB} = 20 \log \left( \frac{4\pi r}{\lambda} \right) - 20 \log F, \quad (2)$$

where  $r$  is the range and  $\lambda$  is the wavelength. The first term in Equation (2) is the free-space loss and all environmental effects, including troposcatter, are contained in the propagation factor,  $F$ . The terms “signal strength” and “received power” at the antenna will be used interchangeably for the remainder of this report.

Based on real-time meteorological measurements made in the California and Arizona desert described in Reference [15], surface-based ducts measured were attributable to thermal cooling of the desert floor; therefore, any variation in duct height tended to follow the variation in terrain elevation along the path. Based on these real-time meteorological measurements, and for the sake of thoroughness, we applied the refractivity profiles from soundings and climatology in two ways. First, the soundings and profiles constructed from climatology were applied and referenced to mean sea level for all terrain paths. For the second method, we applied the refractivity profiles relative to the local ground height along the path such that any trapping layers, whether at the surface or elevated, would follow the terrain elevation along each propagation path. Lastly, signal strength predictions were also obtained for standard atmosphere conditions for baseline comparisons.

Results from the widely used terrain diffraction model TIREM (Version 3.02) are also presented here as an additional comparison of model performance. TIREM uses a combination of spherical earth and knife-edge diffraction algorithms to compute the propagation loss between point-to-point terminals. TIREM does not allow for vertically varying refractive profiles and assumes a linear gradient; therefore, standard atmosphere was used for all TIREM results. A nominal surface refractivity value of 301.0 required for TIREM was applied along with USGS terrain data. The remaining applicable parameters used for TIREM are identical to those used for the APM.

## A. WXL-87 (YUMA)

We begin the analysis with signal strength data collected from the WXL-87 transmitter. Of the two data sets, this set contains longer propagation paths, but meteorologically speaking, is the least uneventful of the two sets. Figure 10 shows a time series plot of the observed signal on 09 June 2004, along with predictions from the APM. The solid colored lines indicate the APM predictions corresponding to the various refractivity profiles used from soundings and climatology, along with standard atmosphere conditions. Only one sounding was available for this day, so there is no distinction between daytime or nighttime soundings. Predictions shown in the top plot of Figure 10 are predictions using USGS data and predictions shown in the bottom plot were computed using DTED terrain information. The start and end times correspond to roughly the same geographic location, which is shown as the westernmost portion of the magenta curve in Figure 2. The time at which the vehicle reached its easternmost location on the receiver route and reversed direction can easily be seen at hour 18.25, where the signal strength reached its peak. This peak corresponds to the time at which the vehicle was nearest to the transmitter. From hour 18.25 onward, the vehicle collected data as it was traveling westward, which is illustrated by an almost “mirror-like” variation in signal strength centered at hour 18.25 as measurements were made on the same route but in the opposite direction.

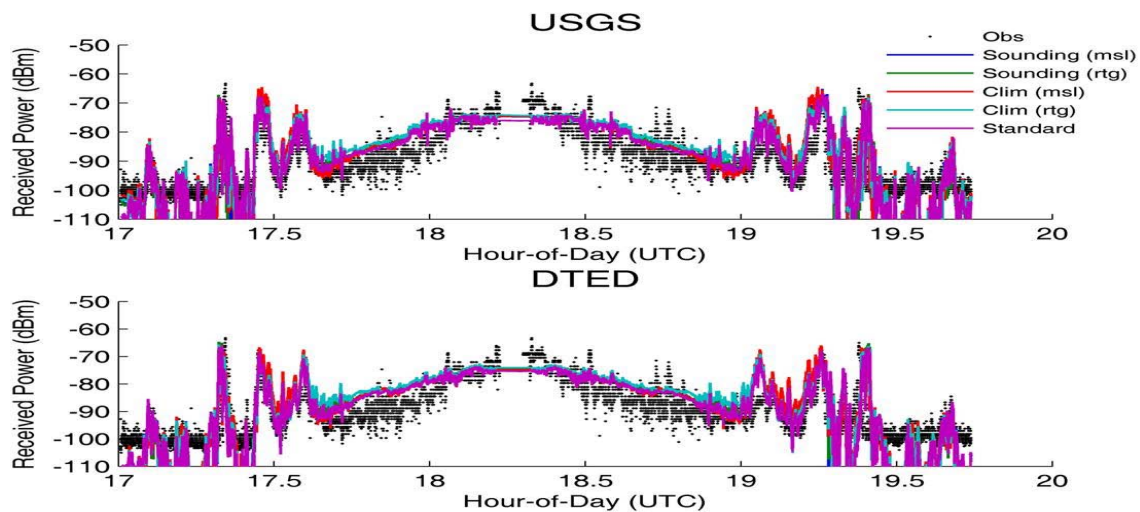


Figure 10. Observed signal strength from WXL-87 transmitter on 09 June 2004 and APM predictions for various profiles from sounding and climatology (solid colored lines) using terrain information from USGS (top) and DTED (bottom).

Only data collected on 09 June 2004 is shown for this transmitter, as these data are fairly representative of the qualitative comparison between measurements and predictions for all 10 measurement days. What is apparent is that predictions made using actual soundings obtained at the nearest meteorological station (1Y7) were almost identical to those using standard atmosphere, although this could have been surmised from the height/M-unit profiles shown in Figure 6. Predictions made using climatology, where surface-based duct profiles were generated, were also not very different than those generated under standard atmosphere conditions. Qualitatively, there appears to be no significant difference between the APM predictions based on DTED and those obtained using USGS. This finding is consistent with Figure 8b, which shows that DTED terrain elevation did not differ greatly from USGS terrain for most of the path along this receiver route.

In obtaining a quantitative description of the performance of the APM for all 10 measurement days, we first look at the root mean square (RMS) error between predicted and observed signal strength. The RMS error is defined as

$$E_{rms} = \sqrt{\frac{\sum_{i=1}^m [P_{r\_obs}(i) - P_r(i)]^2}{m}}, \quad (3)$$

where  $P_{r\_obs}$  represents the observed received power at the antenna,  $m$  is the number of observations, and  $P_r$  represents predictions obtained from the APM with varying terrain and refractivity combinations.

Figure 11 shows the RMS error between observations and the APM predictions using only USGS data with varying refractivity profiles based on soundings, climatology, and standard atmosphere. The refractivity profiles applied relative to mean sea level are indicated by the solid line and those applied relative to the local ground height are shown by the dashed line. Both daytime and nighttime soundings were used to obtain predictions, although for the 1Y7 station, only 2 days contained soundings at 1100 PDT. The RMS error obtained using these soundings is indicated by the red dots. Over the entire collection period, the RMS error varied between roughly 6 and 13 dBm. There is no significant difference in the APM's performance based on actual soundings and climatology, or in how the refractivity profiles are applied. Simply using a standard atmosphere resulted in slightly better agreement with observations.

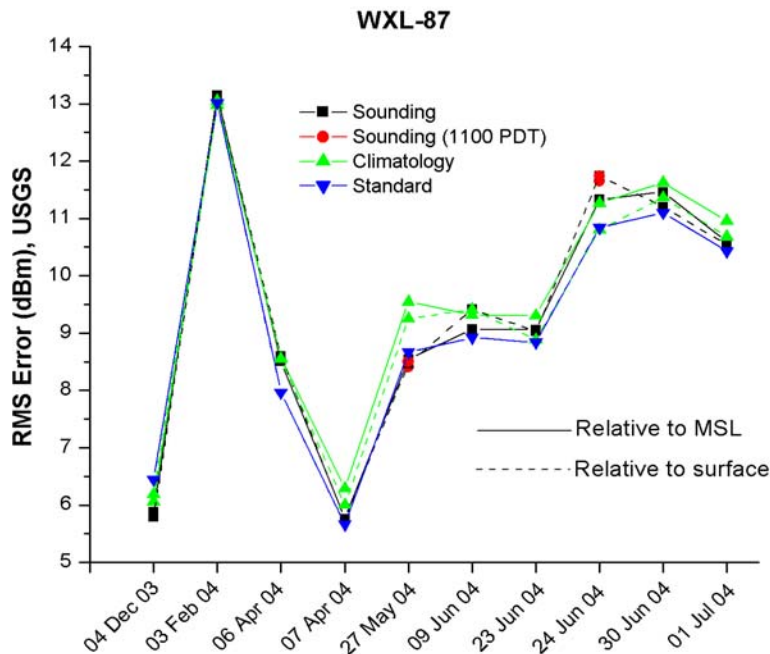


Figure 11. RMS error between measurements and APM predictions for each measurement day for the WXL-87 transmitter. APM predictions were obtained based on USGS terrain data, and refractivity profiles are applied relative to mean sea level (solid line) and relative to the ground height along the path (dashed line).

Table 3 lists the numerical values of RMS error and standard deviation, in dBm, between observations and APM predictions using USGS terrain and refractivity profiles based on soundings, climatology, and standard atmosphere. The table also lists the RMS error and standard deviation between observations and TIREM predictions using standard atmosphere. The APM RMS error values in Table 3 are for predictions where the refractivity profiles were applied relative to the local ground height. The RMS error for refractivity profiles applied relative to mean sea level are similar (to within 1 dBm), so they are not listed separately. Both daytime and nighttime soundings were used to obtain predictions, although for the 1Y7 station, only 2 days contained soundings at 1100 PDT. For days 27 May 2004 and 24 June 2004, a second value is listed corresponding to the second sounding available for these 2 days at 1100 PDT. Comparison between TIREM and the APM results (standard atmosphere columns) shows that TIREM provides roughly 2 to 4 dBm higher RMS error than the APM. TIREM also shows more variability in its predictions, resulting in an even higher standard deviation than the APM of roughly 2 to 6 dBm.

Table 3. WXL-87 (USGS terrain).

Day	RMS Error (dBm)				Standard Deviation (dBm)			
	APM			TIREM	APM			TIREM
Sounding	Climatology	Standard	Standard	Sounding	Climatology	Standard	Standard	
04 Dec 03 <sup>a</sup>	5.8	6.2	6.4	9.2	5.6	6.0	6.4	24.1
03 Feb 04	13.1	13.0	13.0	14.6	11.7	12.2	11.9	12.6
06 Apr 04	8.6	8.5	8.0	9.8	8.5	8.4	7.9	13.6
07 Apr 04	5.7	6.0	5.7	8.5	5.7	5.8	5.7	13.5
27 May 04	8.5 / 8.5	9.2	8.7	11.3	8.4 / 8.4	9.2	8.6	15.5
09 Jun 04	9.4	9.4	8.9	11.2	9.4	9.3	8.9	16.2
23 Jun 04	9.0	8.9	8.8	12.7	7.6	8.4	7.9	15.7
24 Jun 04	11.7 / 11.7	10.8	10.8	13.4	10.9 / 10.0	10.2	9.8	14.7
30 Jun 04	11.2	11.4	11.1	13.5	10.5	11.1	10.6	13.4
01 Jul 04	10.5	10.7	10.4	12.9	10.2	10.6	10.2	16.3

<sup>a</sup>5-s samples

Using different sources of terrain information (or alternatively, different terrain resolutions) has greater impact on the APM predictions. Figure 12 shows the RMS error between observations and the APM predictions using DTED (solid line) and USGS (dashed line) terrain for the various refractivity profiles, similar to Figure 11, but applied relative to the local ground height only. There is decidedly better agreement with measurements for predictions based on USGS terrain. The RMS error based on the APM predictions using USGS varied from 0.7 to 2.9 dBm lower than for predictions using DTED.

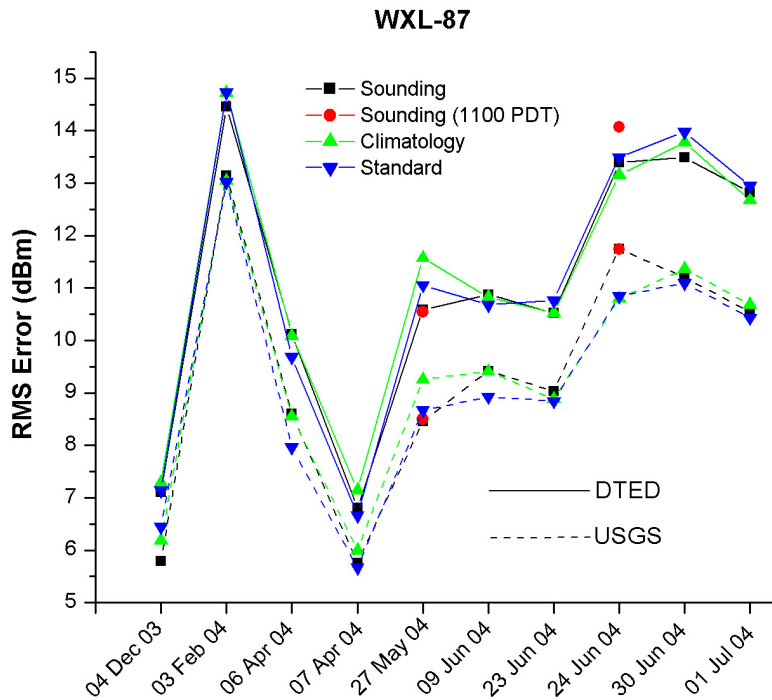


Figure 12. RMS error between measurements and APM predictions for each measurement day for the WXL-87 transmitter. Predictions were obtained using DTED (solid line) and USGS (dashed line) information. All refractivity profiles are applied relative to the local ground height along the path.

Although statistics are provided for each day, another meaningful or more descriptive statistic for communications engineers is how well a particular propagation model performs within a specified confidence interval over time. Eastbound and westbound observations for 9 of the 10 measurement days were used to compute the 95% confidence interval shown in Figure 13. Only day 04 Dec 2003 was excluded due to the lower sampling rate. The shaded area represents the 95% confidence interval based on the 18 data sets and is plotted as a function of range from the transmitter. The black line in Figure 13a represents the mean of the observations. From Table 3, Figure 11, and Figure 12, predictions based on standard atmosphere performed statistically as well as those based on climatology and actual soundings. Also, the APM performed noticeably better (i.e., lower RMS error) with USGS terrain than with DTED terrain. Therefore, what is shown by the black curve in Figure 13b is the mean of the APM predictions over the 9 measurement days using standard atmosphere and USGS terrain. Figure 13c shows the corresponding TIREM results, also for standard atmosphere and USGS terrain. From a visual comparison of Figure 13b and Figure 13c, the higher variability from TIREM is evident, with some portions of the predicted signal strength falling well outside the confidence interval.

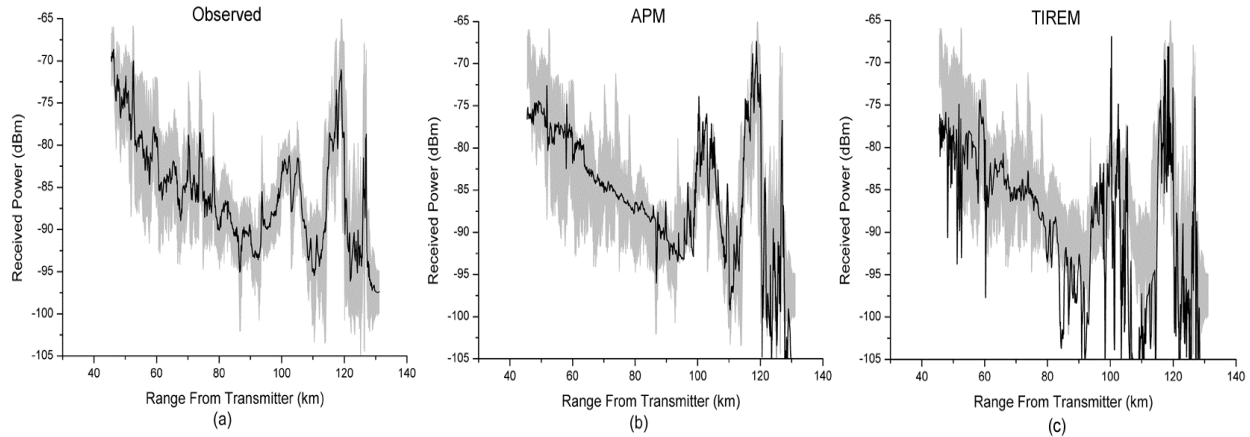


Figure 13. 95% confidence interval of observations (shaded area in all plots) along with (a) the observed mean, (b) the APM predictions, and (c) the TIREM predictions (all shown as black lines) from the WXL-87 transmitter as a function of range from the transmitter. APM and TIREM predictions based on standard atmosphere and USGS terrain.

Note that along the route, for all 9 measurement days, the proximity of the receiver from the transmitter varied from 40 km to over 130 km, with a dynamic range in signal strength of over 40 dBm. It should be emphasized here that this dynamic range was observed within a span of 2 to 3 hours (time duration varies for each day) as the vehicle traveled east and west at normal highway speeds. The APM performed extremely well in tracking the WXL-87 signal strength over the course of the 80+ km receiver route out to roughly 130 km from the transmitter, where it begins to deviate from observations at the farthest ranges.

## B. KEC-62 (SAN DIEGO)

From Figure 4, the relatively high occurrence of both surface-based and elevated ducts would appear to induce more variable signal strength from the KEC-62 transmitter that cannot be readily explained by standard atmosphere conditions as with the WXL-87 data. Particularly in light of the proximity of the NKX meteorological station to the receiver route (Figure 2), this station would have lent itself to more accurate predictions based on the measured refractivity profiles. However, this was not the case for *most* of the measurement period. The exception will be discussed in detail in Section III.C.

The rugged topography for propagation paths over this route, coupled with the low-altitude receiver, makes diffraction the dominant propagation mechanism, which yields very little impact on the signal strength, due to varying refractivity. See the qualitative comparison between observations and predictions for day 23 Jun 2004 in Figure 14. The first portion of the measurements (from hour 17.5 to 18.5) were obtained as the receiver traveled eastward, and from hour 21.5 onward, the data were collected traveling west. Similar to Figure 10, predictions based on USGS terrain are shown in the top plot and those using DTED are provided in the bottom plot.

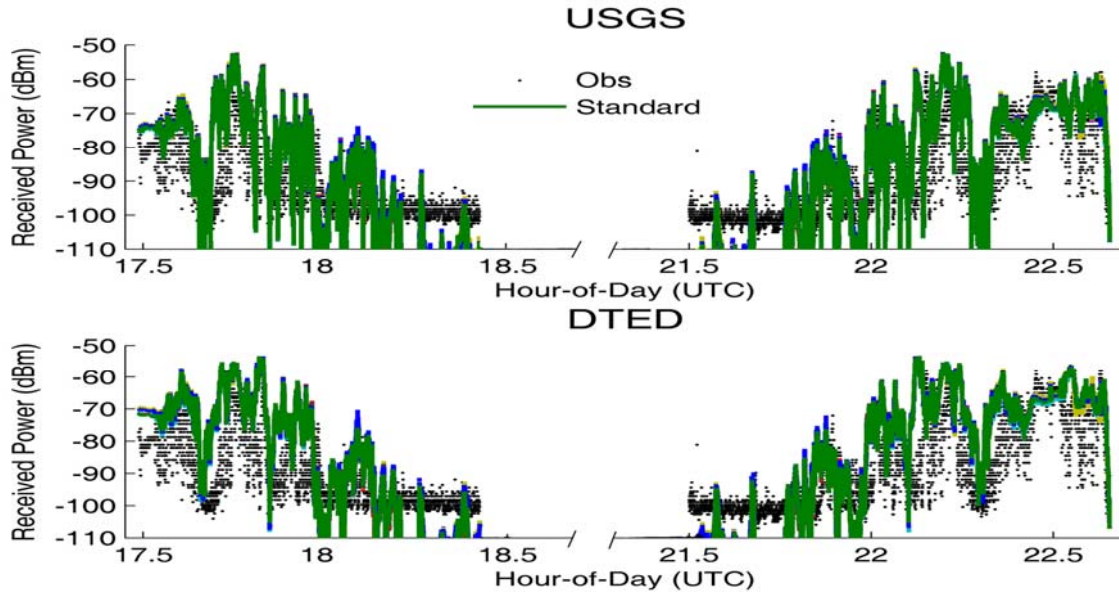


Figure 14. Observed signal strength from the KEC-62 transmitter on 23 June 2004 and the APM predictions for various profiles from soundings, climatology, and standard atmosphere (green line most easily seen) using terrain information from USGS (top) and DTED (bottom).

From Table 2, for all but one collection day, two soundings were available. Along with two soundings per day, we also applied surface-based and elevated ducts constructed from climatology, with standard atmosphere again used as a baseline. As was done with the WXL-87 data, profiles were applied relative to mean sea level and relative to the local ground height. Therefore, Figure 14 shows *nine* different sets of the APM predictions for each plot. Most of these predictions are indistinguishable from the standard atmosphere predictions. After looking more carefully, one can find a hint of slight differences in predictions due to various refractivity profiles. Practically speaking, however, these differences are negligible.

Indeed, the RMS error computed for each day based on the various refractivity profiles vary less than 1 dBm from that for standard atmosphere conditions. This variation is illustrated in Figure 15, where the RMS errors based on profiles applied relative to mean sea level are indicated by the solid line and those applied relative to the local ground height are shown by the dashed line. The RMS error for the first day (04 Dec 2003) is significantly larger due to the difference in time sampling of the signal strength (Section II.A), which is indicated by the line plotted “off the chart.”

On the other extreme, due to the availability of signal strength data on the westward direction only of the receiver route for day 03 Feb 2004, the RMS error is somewhat lower than the remaining measurement days. Also, on 30 June 2004, only a portion of the data collected on the eastbound and westbound routes are included in the computations for the RMS error and standard deviation, due to limited signal reception of the KEC-62 transmitter. This transmitter is detailed in Section III.C. Again, the various refractivity profiles, whether applied to mean sea level or to the ground height, had no significant impact on the quality of the predictions.

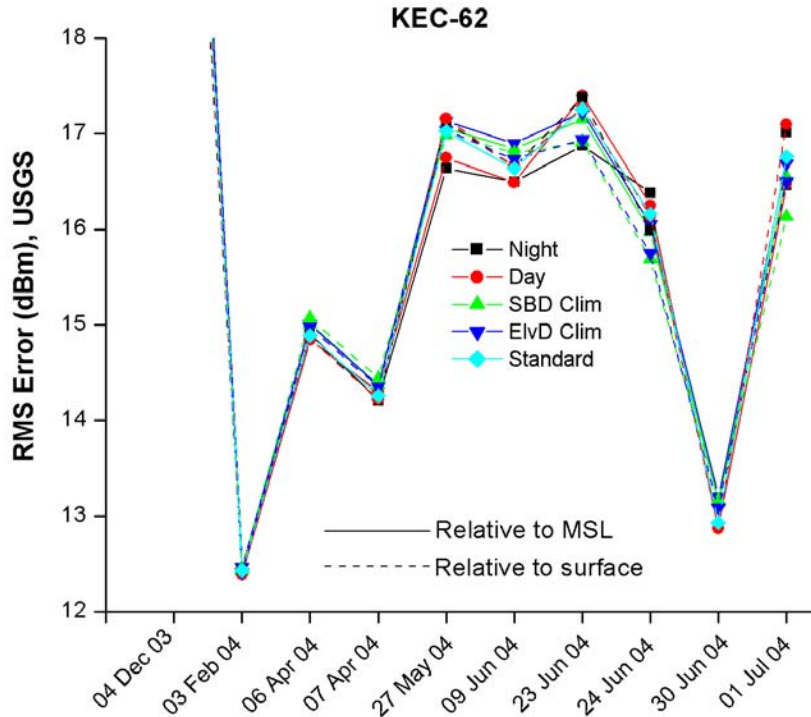


Figure 15. RMS error between measurements and APM predictions for each measurement for the KEC-62 transmitter. APM predictions were obtained based on USGS terrain data, and refractivity profiles are applied relative to msl (solid line) and relative to the local ground height along the path (dashed line).

The difference in predictions based on USGS and DTED terrain data are noticeable. Figure 8a shows that for this portion of the receiver route, differences in terrain elevation between the two databases are significant. It should be emphasized that these differences are shown only at the receiver location as it traveled east and west, plotted as a function of distance from the transmitter. Based on the surrounding topography shown in Figure 2, the discrepancies shown in Figure 7 also suggest large differences in elevation along each terrain path between the transmitter and the latitude/longitude receiver point.

Figure 16 shows the RMS error for the APM predictions based on USGS and DTED terrain. The APM predictions used to obtain the RMS error are based on all nine refractivity profiles but applied relative to the ground height only. Predictions based on USGS terrain resulted in errors from 1 to 4 dBm lower than predictions based on DTED. Table 4 and Table 5 list the RMS error and standard deviation, respectively, between measurements and the APM predictions for all refractive profiles for USGS terrain. The corresponding TIREM RMS error and standard deviation are listed in the last columns of each table. For these propagation paths, the TIREM results are generally lower in RMS error than the APM results shown in Table 4 by 0.5 to 1.6 dBm. However, the standard deviation results are somewhat mixed in that TIREM results are 2 to 3 dBm higher than the APM (Table 5) for some measurement days, while on other days, TIREM shows a 2-dBm lower standard deviation.

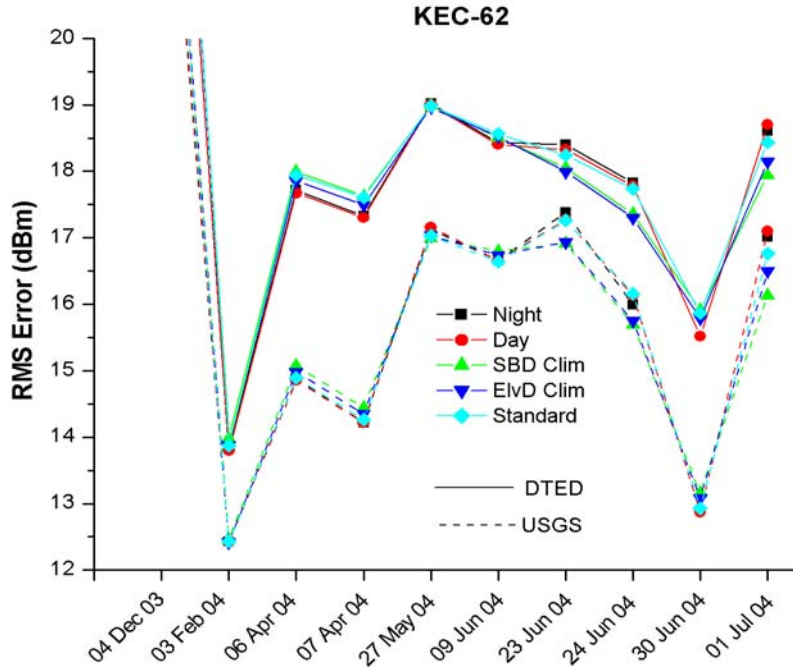


Figure 16. RMS error between measurements and the APM predictions for each measurement day for the KEC-62 transmitter. Predictions were obtained using DTED (solid line) and USGS (dashed line) information. All refractivity profiles are applied relative to the local ground height along the path.

Table 4. KEC-62 APM RMS error in dBm (USGS terrain, refractivity applied relative to ground).

Day	Night Sounding	Day Sounding	Climatology Surface-Based Duct	Climatology Elevated Duct	Standard	TIREM RMS Error
04 Dec 03 <sup>a</sup>	24.4	24.6	25.2	25.5	25.1	24.1
03 Feb 04	12.4	12.4	12.4	12.4	12.4	12.6
06 Apr 04	14.9	14.8	15.1	14.9	14.9	13.6
07 Apr 04	14.2	14.2	14.4	14.3	14.3	13.5
27 May 04	17.1	17.1	17.0	17.0	17.0	15.5
09 Jun 04	16.6	16.6	16.8	16.7	16.6	16.2
23 Jun 04	17.4	17.3	16.9	16.9	17.2	15.7
24 Jun 04	16.0	16.1	15.7	15.7	16.2	14.7
30 Jun 04	-	12.9	13.2	13.1	12.9	13.4
01 Jul 04	17.0	17.1	16.1	16.5	16.8	16.3

<sup>a</sup>5-s samples

Table 5. KEC-62 APM standard deviation in dBm (USGS terrain).

Day	Sounding Night	Sounding Day	Climatology			TIREM Standard Deviation
			Surface-Based Duct	Elevated Duct	Standard	
04 Dec 03 <sup>a</sup>	24.2	24.4	24.9	25.1	24.8	22.8
03 Feb 04	12.1	12.2	12.1	12.1	12.1	12.5
06 Apr 04	10.7	10.8	10.7	10.7	10.7	12.8
07 Apr 04	9.8	9.8	9.7	9.7	9.7	12.7
27 May 04	16.8	16.8	16.6	16.7	16.7	15.5
09 Jun 04	12.2	12.2	11.8	11.8	12.0	14.0
23 Jun 04	17.4	17.3	16.9	16.9	17.3	15.2
24 Jun 04	15.9	16.2	15.7	15.7	16.1	13.9
30 Jun 04	-	10.4	10.3	10.4	10.4	13.4
01 Jul 04	16.9	17.0	16.1	16.5	16.7	15.5

<sup>a</sup>5-s samples

Providing a similar comparison as in the previous section, Figure 17 shows the 95% confidence interval for 9 days of observations along the KEC-62 receiver route, along with the mean. To avoid displaying signal strength for duplicate ranges corresponding to different coordinates on the receiver route, the data collected on this receiver path are split into those collected on that portion west (Figure 17a) and east (Figure 17b) of the transmitter indicated by the red and black curves, respectively, shown in Figure 9.

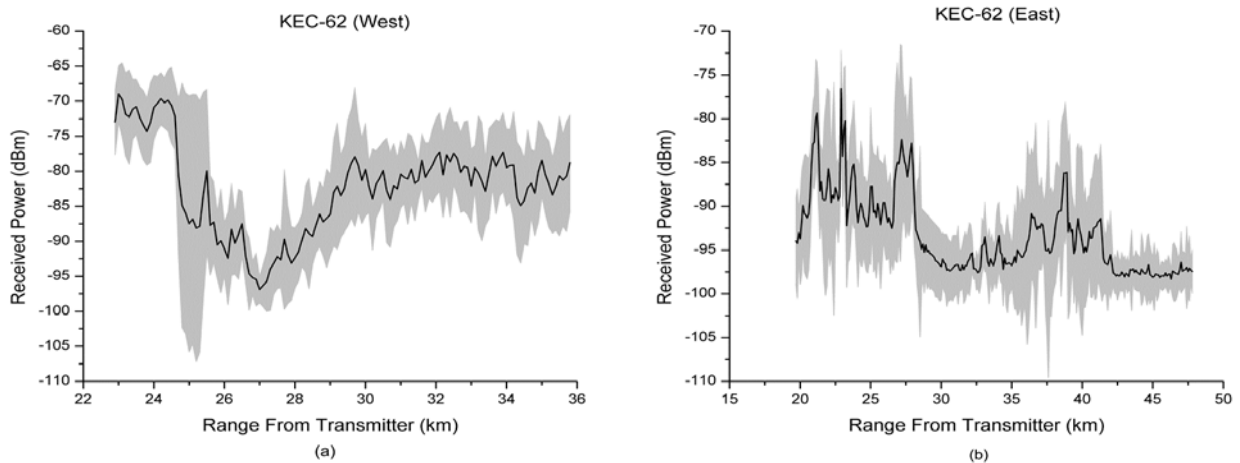


Figure 17. 95% confidence interval (shaded area) and mean (black line) of observations from the KEC-62 transmitter for portions of the receiver route (a) west and (b) east of the transmitter, indicated by the red and black curves, respectively, shown in Figure 9.

Figure 18 shows the mean of the corresponding APM predictions. Again, because the predictions based on standard atmosphere did not differ greatly from those based on soundings or climatology, predictions shown in Figure 18 are based only on standard atmosphere and USGS terrain. The RMS error for the entire route is higher than that for the WXL-87 data and varied from 12.4 to 17.2 dBm (excluding day 04 Dec 2003). The higher overall error is apparently due to the relatively poor agreement between the APM and observations along the western portion of the receiver route, which corresponds to shorter ranges from the transmitter of between 23 and 36 km. Along the eastern portion of the route, the APM showed better agreement (Figure 18b), although not to the extent shown in Figure 13.

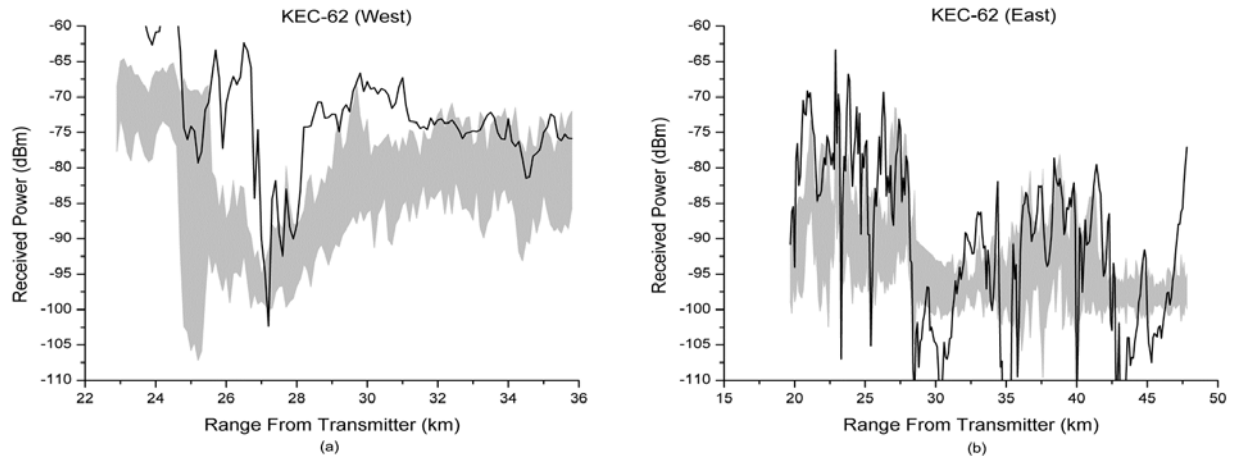


Figure 18. 95% confidence interval as in Figure 17 (shaded area), along with the mean of the APM predictions (black line) for the KEC-62 transmitter for portions of the receiver route (a) west and (b) east of the transmitter, based on standard atmosphere and USGS terrain.

Figure 19 shows the corresponding mean of the TIREM predictions for the east and west portions of the route, similar to Figure 17. For the west portion of the route, TIREM shows a similar over-prediction of signal strength as the APM for ranges from 23 to 27 km. Beyond 27 km, TIREM shows overall better agreement than the APM. On the east portion of the route, TIREM shows generally good agreement, although because of the high variability, tends to “straddle” the confidence interval, with high and low signal strength falling proportionately outside the interval.

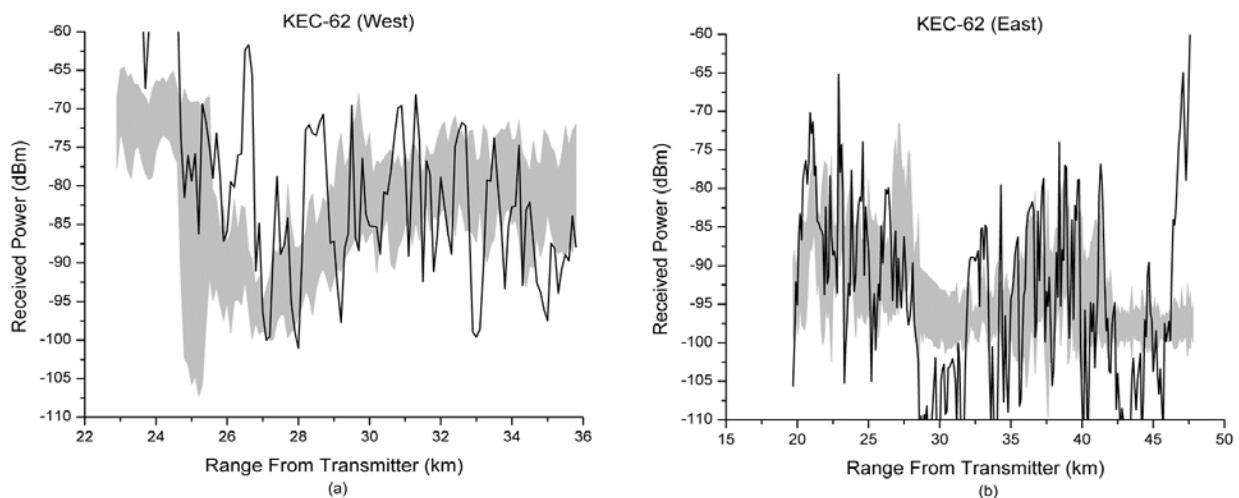


Figure 19. 95% confidence interval as in Figure 17 (shaded area), along with the mean of the TIREM predictions (black line) for the KEC-62 transmitter for portions of the receiver route (a) west and (b) east of the transmitter, based on standard atmosphere and USGS terrain.

As mentioned previously, on 30 June 2004, the APM results provided one of the lowest RMS errors, which is most likely attributable to a smaller number of observations from the KEC-62 transmitter (similar to day 03 Feb 2004). The reason for the limited KEC-62 data on this day is due to an interesting incident described in the next section.

### C. 30 JUNE 2004

On this day, while traveling eastward and recording radio signals from the KEC-62 transmitter, we received interference from an alternate NOAA weather radio station located in Santa Barbara (call sign KIH-34, coordinates 34N 31' 31"/119W 57' 29"). The KIH-34 transmitter antenna height is 1240.2 m above mean sea level and operates at the same frequency of 162.4 MHz as the KEC-62 transmitter, but with a higher power output of 330 W. Within a span of 2 to 3 min after the start of receiving mixed interference, the KIH-34 transmitter was the dominant radio signal received along our normal receiver route, which was evidenced by the very strong voice reception of the station call sign during normal monitoring within the vehicle. The KIH-34 signal was received for approximately 20 to 25 min on the eastward direction of the route. On the return portion traveling westward, the KIH-34 signal once again came in very strong at roughly the same location as on the eastward direction. The time at which it was received traveling west was 3.5 to 4 hours *after* it was originally received traveling east, indicating that environmental conditions causing this phenomenon persisted for some time. Figure 20 shows the geographic area of southern California, along with the location of the KEC-62 and KIH-34 transmitters in San Diego and Santa Barbara, respectively. The normal receiver route (Interstate 8) is indicated by the white and magenta curve; however, that portion in magenta shows the area where the KIH-34 signals were dominant for this day.

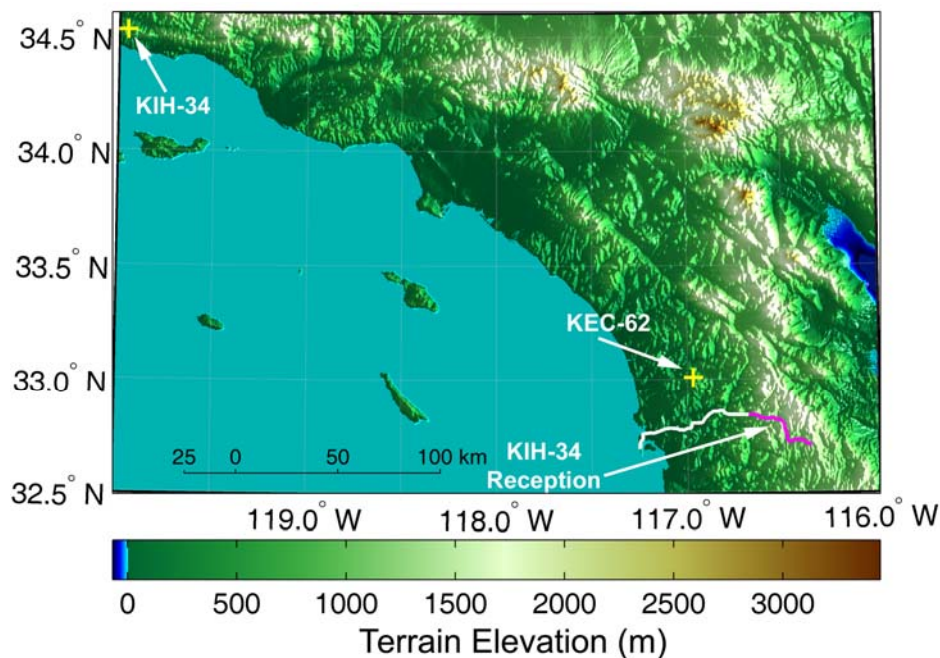


Figure 20. Southern California coastal area showing locations of KIH-34 (Santa Barbara) and KEC-62 (San Diego) transmitters. Magenta portion of the receiver route indicates where KIH-34 transmissions were received on 30 June 2004.

The only day of the 10 measurement days in which we recorded such an event was 30 June 2004. As a qualitative comparison of signal strength observed over this portion of the receiver route, the signal strength recorded from the KIH-34 and KEC-62 transmitters is shown in Figure 21 (eastward direction only). The signal strength observed from the KEC-62 transmitter is a subset of that shown in Figure 14 from hour 18 to 18.5 on 23 June 2004 (which is fairly representative of the signal strength recorded on the other measurement days, except 30 June 2004). The times for both signals have been adjusted such that time 0.0 corresponds to the start of clear KIH-34 reception and the overall time span of 20 to 25 min of observations for both signals correspond to the same GPS latitude/longitude coordinates along the receiver route (that portion in magenta in Figure 20). Clearly, during the first 5 min in Figure 21, much stronger signals were observed on 30 June 2004. During the remaining time where signals were fairly consistent, the mean signal level (from 6 min onward) was roughly 2 dBm higher on 30 June 2004 than on 23 June 2004—not considered significant, yet sufficient enough to receive strong voice quality reception from the KIH-34 transmitter over the geographically closer KEC-62 transmitter.

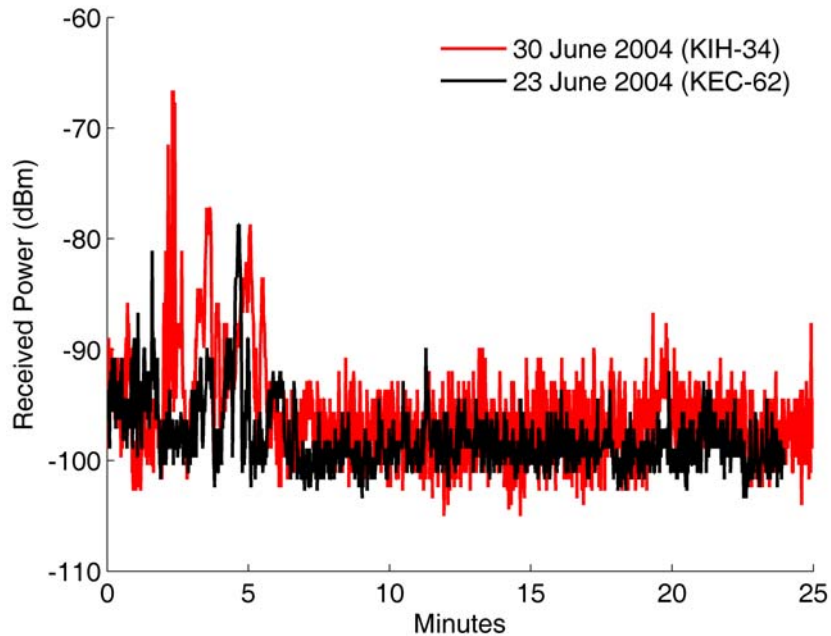


Figure 21. Signal strength received on 23 June 2004 from the KEC-62 transmitter (black) and on 30 June 2004 from the KIH-34 transmitter (red) along the identical portion of the receiver route (magenta curve in Figure 20).

In attempting to explain or account for these higher signal levels, the APM was again used to obtain predictions based on the transmitter/receiver terminals from KIH-34 to the receiver route shown in Figure 20. The ranges for these propagation paths are from 356 to 390 km. Unfortunately, the USGS data readily available for most of the Los Angeles metropolitan area is in the 10-m horizontal resolution format, not in the 30-m horizontal resolution format used in the results already presented. Since we could not merge USGS quadrangles of different formats, we relied only on DTED terrain for these paths.

Another limitation was the lack of real-time atmospheric soundings at locations along the coast from Santa Barbara to San Diego. The only soundings available on 30 June 2004 were from the VBG meteorological station located at Vandenberg (34N 45°/120W 34'), which is near the KIH-34

transmitter site. Soundings were available at 0500 and 1700 PDT. The soundings from both the VBG and NKX meteorological stations for this day are shown plotted to mean signal level in Figure 22. Note that the VBG 0500 PDT sounding shows a strong elevated duct between 1000 and 1350 m, which places the KIH-34 transmitting antenna well within this duct. The VBG sounding at 1700 PDT shows the existence of a duct as well, although at a more elevated height. However, the sounding at NKX, which lies along the propagation paths from the KIH-34 transmitter to the receiver coordinates in question, shows the existence of an elevated but somewhat weaker duct at roughly the same height as the VBG 0500 PDT sounding—indicating that atmospheric conditions were fairly persistent.

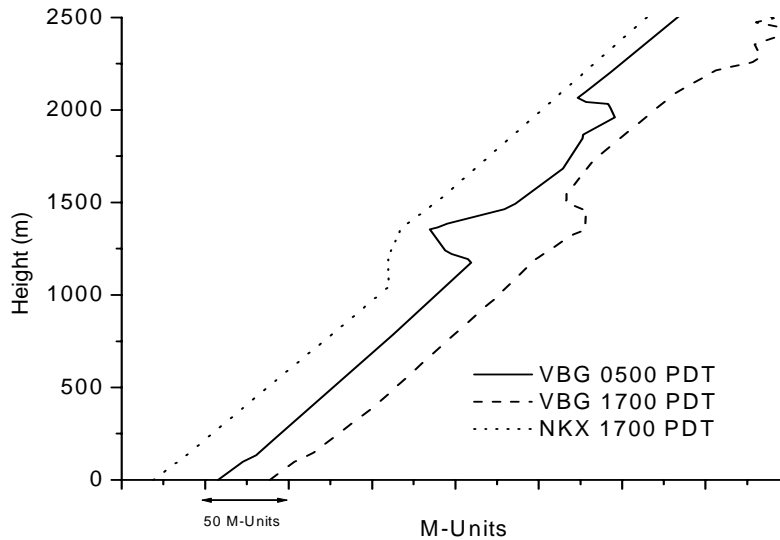


Figure 22. Miramar (NKX) and Vandenberg (VBG) soundings for 30 June 2004.

Figure 23 shows observations for this day and predicted signal strength for all three soundings based on DTED terrain. Qualitatively, the APM was able to predict the higher signal strength observed during the first few minutes; however, it could not adequately track the signal during the remaining time the KIH-34 signal was observed. Predictions using standard atmosphere conditions were also computed for these long propagation paths; however, they were much lower than the minimum of  $-110$  dBm in Figure 23. The lowest RMS error between the KIH-34 observed and predicted signal is based on the VBG 0500 PDT sounding. Using both the eastbound and westbound collected signals, the RMS error is 29.9 dBm.

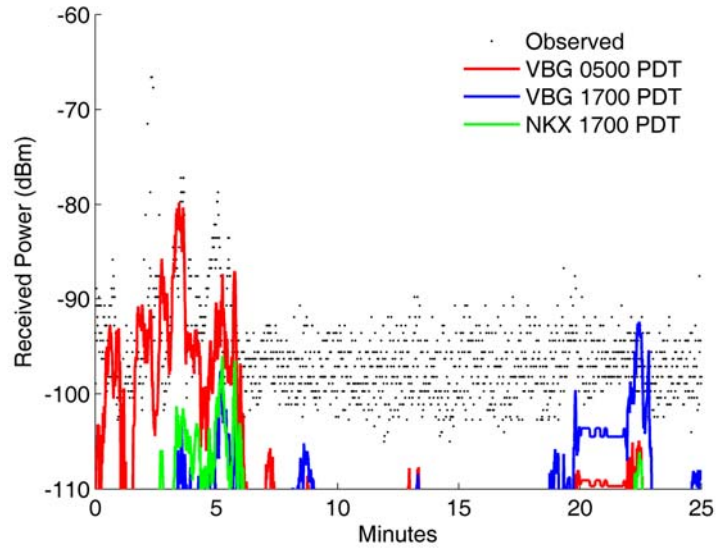


Figure 23. KIH-34 observed signal strength on 30 June 2004 and predictions from the APM using VBG and NKX soundings and DTED terrain.

TIREM results fall well below the  $-110$  dBm vertical minimum shown in Figure 23 for these long propagation paths, which, of course, is expected, as a user can apply only a linear gradient and results are similar to the APM under standard atmosphere conditions for these paths. The fact that the APM was able to account for the KIH-34 reception during the first few minutes based on the VBG sounding proves that anomalous conditions were present.

## IV. DISCUSSION

In all the APM predictions, the surface electrical characteristics were assumed constant with nominal values of 15.0 for the relative permittivity and conductivity of 0.00287 (S/m). Of course, altering the dielectric constants had little to no effect. Based on results presented in Section III.A and Section III.B, also varying the refractive conditions had little effect of statistical significance—not so for the signals measured from the KIH-34 transmitter on 30 June 2004. Simple standard diffraction was not sufficient to account for these signals. From well-established literature on the subject of low-altitude propagation over terrain at VHF and higher frequencies [20]–[22], standard diffraction is considered the dominant propagation mechanism; however, based on the 30 June 2004 observations and the data described in Reference [15], standard diffraction cannot *always* be assumed.

The terrain resolution, or more precisely, the accuracy of the terrain elevation, apparently has a greater impact on the quality of the predictions. As shown in Section III.A, for the WXL-87 receiver route, the RMS error using USGS terrain differed from that using DTED by roughly 2 dBm. The difference in RMS error between the two terrain databases over the more rugged and sharply varying KEC-62 route was on average twice as much. This difference is shown graphically in Figure 16 (refractivity profiles applied to the local ground height), where the dramatic difference in results between the two terrain sources is obvious.

DTED Level 1 has been available for many years and is the database most commonly used within the military. DTED Level 2 is roughly equivalent in horizontal and vertical resolution to the USGS DEM data used in this analysis; however, previous to the Shuttle Radar Topography Mission (SRTM) [23], DTED Level 2 data for much of the world was relatively sparse due to the labor-intensive method of data collection at the time. With the SRTM data now available in DTED Level 2 format, it is expected that errors shown in Section III from the APM will be consistent with those provided by USGS data and any large discrepancies can then be isolated as resulting from the propagation model itself rather than coupled with the source of the terrain information.

Based on the higher resolution USGS data, the APM performed very well, particularly for the longer paths from the WXL-87 transmitter. Based on the comparisons with the KEC-62 data, the APM appears to perform better for longer paths than for shorter paths, as seen in Figure 18a, with the poorest agreement shown for the shortest paths west of the KEC-62 transmitter. The fact that the APM agreed very well with the WXL-87 data over what is predominantly low-lying (i.e., not very rugged) desert, and did not agree very well with the KEC-62 data, where most of the terrain paths are fairly rugged, initially led us to conclude that the APM had basic limitations on its applicability to rugged, steep terrain. However, the propagation paths comprising the eastern portion of the KEC-62 receiver route consist of much more rugged terrain than the western portion, yet the APM showed better agreement over the east portion of the route, as shown in Figure 18b.

The overall RMS error based on USGS terrain for the WXL-87 route was less than 10 dBm for over half the measurement days, while the error varied from 12.4 to 17.2 dBm (excluding day 04 Dec 2003) for the KEC-62 route. Although the KEC-62 receiver route corresponds to shorter ranges from the transmitter and may be less susceptible to cumulative errors associated with longer propagation paths, not accounting for vegetation and localized urban effects may have led to the over-estimation of signal strength. To include vegetation effects on radiowave propagation within the

context of the PE algorithm is a complex problem and is a topic for further study.

The purpose of including TIREM in this analysis is simply for thoroughness in comparing the performance of the APM to the performance of what is generally considered a standard model for propagation over terrain. For low-altitude propagation over most of the measurement days, the analysis shows that the APM performed at least as well as TIREM; however, TIREM could not account for the signals received from the KIH-34 transmitter on 30 June 2004 due to its basic limitations. In civilian or military operational applications that may be used for communications planning purposes, a fast, yet limited model may be perfectly suitable as the need may usually be to establish a communications link with a specified quality-of-service. However, for specialized military applications such as signal intelligence or special warfare, the ability to exploit environmental conditions such as existed on 30 June 2004 would be extremely advantageous, not only for positioning for optimum signal interception, but also to avoid signal interception.

## V. CONCLUSION

The analysis provided in this report shows that a well-established radiowave propagation model, APM, performs very well for low-altitude propagation over terrain. Other widely used terrain models ignore anomalous atmospheric conditions, and as shown in Section III.C, anomalous propagation effects *can* occur. A high-fidelity propagation model is necessary to account for many effects caused by the environment, particularly in areas of the world where refractivity effects over land are just as important as variations in terrain elevation. While a parabolic equation model may not *always* be necessary for low-altitude diffraction over terrain, the APM performs at least as well as the widely used diffraction model, TIREM, under standard conditions, and shows better performance when variable refractivity data are available.

Ultimately, the performance of *all* radiowave propagation models are fundamentally limited by the quality of environmental information available to make adequate field strength estimates. However, as shown by the data on 30 June 2004, even a minimum of meteorological information can help explain some of the received anomalous signals. With the development of the APM, which can now account for many environmental effects over water, land, and coastal regions for both surface and airborne emitters, any electromagnetic assessment tool has the capability to incorporate a single unified model for operational use within various environments.

## VI. REFERENCES

- [1] M. Meeks. 1983. "VHF Propagation over Hilly, Forested Terrain," *IEEE Transactions on Antennas and Propagation*, vol. 31, no. 33 (May), pp. 483–489.
- [2] S. Ayasli. 1986. "SEKE: A Computer Model for Low Altitude Radar Propagation over Irregular Terrain," *IEEE Transactions on Antennas and Propagation*, vol. 34, no. 8 (Aug), pp. 1013–1023.
- [3] R. J. Leubbers. 1984. "Propagation Prediction for Hilly Terrain using GTD Wedge Diffraction," *IEEE Transactions on Antennas and Propagation*, vol. 32, no. 9 (Sep), pp. 951–955.
- [4] K. Chamberlin and R. Leubbers. 1982. "An Evaluation of Longley-Rice and GTD Propagation Models," *IEEE Transactions on Antennas and Propagation*, vol. 30, no. 6 (Nov), pp. 1093–1098.
- [5] L. T. Rogers. 1996. "Effects of the Variability of Atmospheric Refractivity on Propagation Estimates." *IEEE Transactions on Antennas and Propagation*, vol. 44, no. 4 (Apr), pp. 460–465.
- [6] J. H. Richter and H. V. Hitney. 1975. "The Effect of the Evaporation Duct on Microwave Propagation," Naval Electronics Laboratory Center\* TR 1949 (Apr), San Diego, CA.
- [7] K. D. Anderson. 1995. "Radar Detection of Low Altitude Targets in a Maritime Environment," *IEEE Transactions on Antennas and Propagation*, vol. 43, no. 6 (June), pp. 609–613.
- [8] A. E. Barrios. 1992. "Parabolic Equation Modeling in Horizontally Inhomogeneous Environments," *IEEE Transactions on Antennas and Propagation*, vol. 40, no. 7 (July), pp. 791–797.
- [9] A. E. Barrios. 1995. "Terrain and Refractivity Effects in a Coastal Environment: Results from the VOCAR Experiment," *11<sup>th</sup> Annual Review of Progress in Computational Electromagnetics* (pp. 784–789). 20–25 March. Naval Postgraduate School, Monterey, CA, Institute of Electrical Engineers.
- [10] A. E. Barrios, "Terrain and Refractivity Effects in a Coastal Environment," AGARD SPP Symposium on Propagation Assessment in Coastal Environments, Advisory Group for Aerospace Research and Development, AGARD CP-597 (Sep), NASA Center for Aerospace Information, Linthicum MD.
- [11] H. V. Hitney and R. Vieth. 1990. "Statistical Assessment of Evaporation Duct Propagation," *IEEE Transactions on Antennas and Propagation*, vol. 38, no. 6 (June), pp. 794–799.
- [12] K. D. Anderson. 1989. "Radar Measurements at 16.5 GHz in the Oceanic Evaporation Duct," *IEEE Transactions on Antennas and Propagation*, vol. 37, no. 1 (Jan), pp. 100–106.

---

\* now SPAWAR Systems Center San Diego (SSC San Diego)

- [13] J. H. Whitteker. 1994. "Ground Wave and Diffraction." In *Propagation Modeling and Decision Aids for Communications, Radar and Navigation Systems* (pp. 2A-1–2B-13). AGARD Lecture Series 196 (Sep). Advisory Group for Aerospace Research and Development, NASA Center for Aerospace Information, Linthicum MD.
- [14] D. Eppink and W. Kuebler. 1994. "TIREM/SEM Handbook." ECAC-HDBK-93-076 (March), U.S. Department of Defense Electromagnetic Compatibility Analysis Center, Annapolis MD.
- [15] J. P. Day and L. G. Trolese. 1949. "Propagation of Short Radio Waves over Desert Terrain," Naval Electronics Laboratory\* Report 149 (Nov. 3), San Diego, CA.
- [16] A. E. Barrios. 1994. "A Terrain Parabolic Equation Model for Propagation in the Troposphere," *IEEE Transactions on Antennas and Propagation*, vol. 42, no. 1 (Jan), pp. 90–98.
- [17] A. E. Barrios. 2003. "Considerations in the Development of the Advanced Propagation Model (APM) For U.S. Navy Applications." *Proceedings of the International Conference on Radar, RADAR 2003*, 3–5 September 2003, Adelaide, Australia.
- [18] M. F. Levy. 2000. *Parabolic Equation Methods for Electromagnetic Wave Propagation*, IEE Electromagnetic Wave Series 45, London, U.K.
- [19] Electronic Systems Group–Western Division. 1977. "Radiosonde Data Analysis II: Five Years Data." 29 July. GTE Sylvania Incorporated, Mountain View CA.
- [20] H. R. Reed and C. M. Russell. 1964. *Ultra High Frequency Propagation*, Chapman and Hall Ltd., London, U.K.
- [21] M. L. Meeks. 1982. *Radar Propagation at Low Altitudes*, Artech, New York, NY.
- [22] D. E. Kerr. 1951. *Propagation of Short Radio Waves*. MIT Radiation Laboratory Series, McGraw-Hill, New York, NY.
- [23] National Geospatial-Intelligence Agency: <http://www.nga.mil>.

---

\* now SPAWAR Systems Center San Diego (SSC San Diego)

**REPORT DOCUMENTATION PAGE**

*Form Approved  
OMB No. 0704-01-0188*

The public reporting burden for this collection of information is estimated to average 1 hour per response, including the time for reviewing instructions, searching existing data sources, gathering and maintaining the data needed, and completing and reviewing the collection of information. Send comments regarding this burden estimate or any other aspect of this collection of information, including suggestions for reducing the burden to Department of Defense, Washington Headquarters Services Directorate for Information Operations and Reports (0704-0188), 1215 Jefferson Davis Highway, Suite 1204, Arlington VA 22202-4302. Respondents should be aware that notwithstanding any other provision of law, no person shall be subject to any penalty for failing to comply with a collection of information if it does not display a currently valid OMB control number.

**PLEASE DO NOT RETURN YOUR FORM TO THE ABOVE ADDRESS.**

<b>1. REPORT DATE (DD-MM-YYYY)</b> 08-2006		<b>2. REPORT TYPE</b> Final		<b>3. DATES COVERED (From - To)</b>	
<b>4. TITLE AND SUBTITLE</b>  ADVANCED PROPAGATION MODEL (APM) ANALYSIS OF VHF SIGNALS IN THE SOUTHERN CALIFORNIA DESERT				<b>5a. CONTRACT NUMBER</b>	
				<b>5b. GRANT NUMBER</b>	
				<b>5c. PROGRAM ELEMENT NUMBER</b>	
<b>6. AUTHORS</b>  A. E. Barrios K. D. Anderson G. E. Linden				<b>5d. PROJECT NUMBER</b>	
				<b>5e. TASK NUMBER</b>	
				<b>5f. WORK UNIT NUMBER</b>	
<b>7. PERFORMING ORGANIZATION NAME(S) AND ADDRESS(ES)</b> SSC San Diego San Diego, CA 92152-5001				<b>8. PERFORMING ORGANIZATION REPORT NUMBER</b>  TR 1945	
<b>9. SPONSORING/MONITORING AGENCY NAME(S) AND ADDRESS(ES)</b> Office of Naval Research 875 North Randolph Street, Suite 1425 Code 322MM, Processing & Prediction Division Arlington, VA 22203-1995				<b>10. SPONSOR/MONITOR'S ACRONYM(S)</b> ONR 322MM	
				<b>11. SPONSOR/MONITOR'S REPORT NUMBER(S)</b>	
<b>12. DISTRIBUTION/AVAILABILITY STATEMENT</b> Approved for public release; distribution is unlimited.					
<b>13. SUPPLEMENTARY NOTES</b> This is the work of the United States Government and therefore is not copyrighted. This work may be copied and disseminated without restriction. Many SSC San Diego public release documents are available in electronic format at <a href="http://www.spawar.navy.mil/sti/publications/pubs/index.html">http://www.spawar.navy.mil/sti/publications/pubs/index.html</a>					
<b>14. ABSTRACT</b>  This report analyzes very high frequency signal strength data from two Naval Oceanic & Atmospheric Administration weather radio transmitters located in southern California and southwestern Arizona over a wide range of topography ranging from relatively flat to mountainous terrain. Meteorological information was obtained from local radiosonde measurement stations at Miramar (NKX) and Yuma Proving Ground (1Y7). These data are used as the basis for a validation study of the Advanced Propagation Model (APM) to determine its applicability for low-altitude mobile radio communications applications over terrain. The APM performs very well for low-altitude propagation over terrain and at least as well as the widely used diffraction model, Terrain Integrated Rough Earth Model (TIREM), under standard conditions. The APM performs better when variable refractivity data are available.					
<b>15. SUBJECT TERMS</b> Mission Area: Radio Communications propagation modeling      low-altitude propagation      field strength estimation radiowave propagation      meteorological information      signal strength prediction					
<b>16. SECURITY CLASSIFICATION OF:</b>			<b>17. LIMITATION OF ABSTRACT</b>	<b>18. NUMBER OF PAGES</b>	<b>19a. NAME OF RESPONSIBLE PERSON</b>
<b>a. REPORT</b>	<b>b. ABSTRACT</b>	<b>c. THIS PAGE</b>			A. E. Barrios
U	U	U	UU	41	<b>19b. TELEPHONE NUMBER (Include area code)</b> (619) 553-1429

Approved for public release; distribution is unlimited.